

# Morphology of ledge patterns during step flow growth of metal surfaces vicinal to fcc(001)

M. Rusanen<sup>1,2</sup>, I. T. Kopenen<sup>1</sup>, T. Ala-Nissila<sup>2</sup>, C. Ghosh<sup>3</sup>, and T. S. Rahman<sup>3,1</sup>

<sup>1</sup>Department of Physical Sciences, University of Helsinki, P.O. Box 64,  
FIN-00014 University of Helsinki, Finland

<sup>2</sup>Helsinki Institute of Physics and Laboratory of Physics,  
Helsinki University of Technology,

P.O. Box 1100, FIN-02015 HUT, Espoo, Finland

<sup>3</sup>Department of Physics, Kansas State University, Manhattan, KS 66506

The morphological development of step edge patterns in the presence of meandering instability during step flow growth is studied by simulations and numerical integration of a continuum model. It is demonstrated that the kink Ehrlich-Schwoebel barrier responsible for the instability leads to an invariant shape of the step profiles. The step morphologies change with increasing coverage from a somewhat triangular shape to a more flat, invariant steady state form. The average pattern shape extracted from the simulations is shown to be in good agreement with that obtained from numerical integration of the continuum theory.

Epitaxial growth on vicinal surfaces is known to give rise to interesting growth instabilities under suitable conditions, e.g. to step bunching, mound formation and meandering of the step edges<sup>1</sup>. The meandering instability emerges when the interlayer mass transport from the upper side of the step is reduced due to the Ehrlich-Schwoebel barrier<sup>2</sup> enhancing growth of protrusions at the step edges. This is now known as the Bales-Zangwill instability (BZI)<sup>3</sup> which tends to destabilize the ledge morphology due to terrace diffusion and asymmetric interlayer crossing. There is no diffusion along the ledges in BZI. However, recently it was found that in the case of 1+1 dimensional growth there is an analogous phenomenon due to the kink Ehrlich-Schwoebel barrier for going around a kink site at the step edge. The corresponding kink Ehrlich-Schwoebel effect (KESE) leads to growth of unstable structures at the step edges with a dynamically selected wavelength<sup>4</sup>. The ledge instabilities were originally found and reported experimentally on the Cu(1,1,1) vicinal surface<sup>5</sup> but attributed to the BZI scenario. More recent STM experiments on the Cu(1,1,1) surface proposed that the formation of the regular patterns is due to the KESE<sup>6</sup>. Since then theoretical studies of the meandering instability have shown that the KESE indeed supersedes the BZI in the formation of the periodic patterns<sup>4,7,8</sup> and eventually leads to an in-phase motion of the step edge structures<sup>7,8</sup>.

Instability and wavelength selection of the step edge patterns due to the KESE have been studied within the framework of a continuum step model<sup>4</sup>, the solid-on-solid (SOS) lattice model<sup>8,9</sup>, and semi-realistic Monte Carlo

(MC) simulations<sup>7</sup>. In particular, in the recent MC work<sup>7</sup> it was shown that on vicinal Cu(1,1,1) surfaces the observed instability is due to the KESE and the competing BZI is of no importance in the length and time scales considered. The role of dimer nucleation in determining the selected wavelength was confirmed, in good agreement with the theoretical scaling relation<sup>10</sup> and more recent SOS simulations<sup>8</sup>. In the MC simulations, there was evidence of phase locking of the ledge structures at the largest coverages studied, but this was not quantitatively confirmed.

Regarding the step morphologies, a triangular shape has been predicted to occur for a strong KESE and a rounded, more flat shape for a weak KESE<sup>4</sup>. However, the MC simulations of Ref.<sup>7</sup> indicate that in the case of a strong KESE there is in fact an interesting shape transition from narrow, somewhat triangular shapes in the initial stage of growth to more rounded patterns in the large coverage regime. Moreover, the MC simulations of Ref.<sup>7</sup> and SOS model results of Ref.<sup>8</sup> are in disagreement with asymptotic evolution of the step profiles as predicted by the continuum theories<sup>11,12</sup>. In this work we study the ledge morphologies of growing steps on the vicinal Cu(1,1,1) surfaces in detail. In particular, we study the onset of the in-phase growth and the phase-locking of the step profiles in the presence of a strong KESE. Our results show that the ledge morphologies assume an invariant shape due to an interplay between various mass transport currents and phase-locking of the steps. We show how the ledge profiles from the MC simulations can be reproduced by explicitly including the relevant mass transport currents on the surface. On continuum level this indicates a delicate balance between the various currents that determine and stabilize the invariant ledge shapes.

The model system used here is as in Ref.<sup>7</sup>, based on MC simulations of a lattice gas model with energetics from the effective medium theory (for more details, see Refs.<sup>7,13</sup>). Our MC method is efficient enough to simulate growth of Cu up to ten monolayers (ML) under realistic temperature and flux conditions. The temperature range explored here was  $T = 240 - 310$  K and the flux  $F = 3 \cdot 10^{-3} - 1 \cdot 10^{-1}$  ML/s. Thus the ratio between the terrace diffusion and the flux  $D = F \cdot 6 \cdot 10^9 - 10^7$  in units of the lattice constant  $a = 0.255$  nm, corresponding

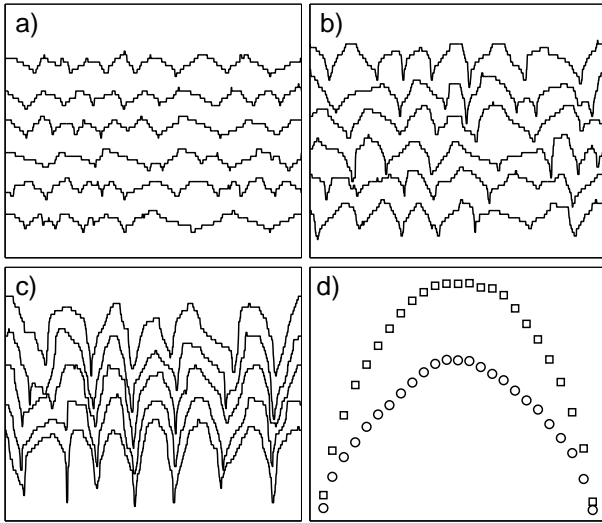


Fig. 1: Snapshots of typical ledge profiles with step orientations in the closepacked [110] direction at  $T = 300$  K with  $F = 8 \cdot 10^{-2}$  ML/s for coverages  $\theta = 0.4; 2.0$ , and  $10.0$ , in figures (a)–(c) (lateral and vertical scales are 1000 and 70 lattice spacings, respectively). In (d) the shape transition is shown, and the profiles have been averaged over the meander periods at  $\theta = 0.4$  ML (circles) and at  $\theta = 2.0$  ML (squares).

to a typical molecular beam epitaxy regime<sup>14</sup>. The energetics of the model also specifies the important length scales controlling step flow growth. These are  $\lambda_c = (12D_s = FL)^{1/4}$ , the length scale for dimer nucleation at the step edge<sup>7,10</sup>,  $D_s$  being the adatom diffusion constant along the straight edge, and the kink Schwoebel length<sup>4</sup>  $\lambda_s = \exp[(E_s - E_d)/k_B T]^{-1}$  which is related to the energy barriers  $E_s = 0.52$  eV and  $E_d = 0.26$  eV for jumps around a kink site and along a straight edge, respectively. For the close packed [110] ledges,  $\lambda_s \sim 10^4$  and  $\lambda_c \sim 10^2$  around room temperature corresponding to strong K ESE<sup>4,8,11</sup>. In Ref.<sup>7</sup> it was shown that the wavelength of the step edge patterns is given by  $\lambda_c$ , with a scaling exponent of about 0.23, and an effective barrier of  $E_e = 75 \cdot 10^{-3}$  eV. Both are in good agreement with the formula for  $\lambda_c$  which gives  $1=4$  and  $E_e = E_d = 4 = 65$  m eV, respectively. Our previous study<sup>7</sup> was done on a Cu(1,1,17) surface but we have checked the results also with smaller terrace widths.

Simulation results for the step edge profiles on Cu(1,1,17) are shown in Figs. 1 (a)–(c) after deposition of  $\theta = 0.4; 2.0$ , and  $10.0$  ML, respectively, at  $T = 300$  K with  $F = 6 \cdot 10^{-2}$  ML/s. In the beginning of growth (Fig. 1 (a)) the shape of the patterns is somewhat triangular as predicted for a relatively strong K ESE<sup>11</sup>. The meandering structures are not yet completely in the same phase indicating that the diffusion field has not yet coupled the subsequent step edge trains, a typical feature for K ESE dominated meandering<sup>8</sup>. However, a selection of the relatively well-defined wavelength for all ledges is apparent already at this stage of growth<sup>7</sup>. At larger coverages the

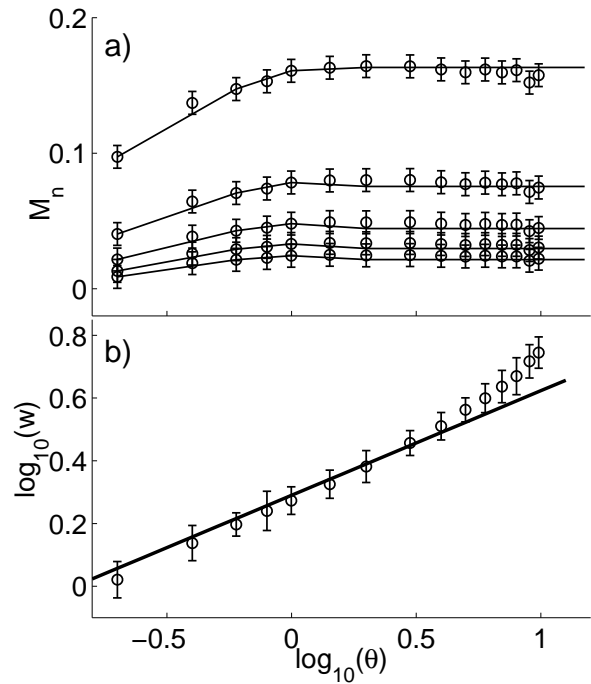


Fig. 2: (a) Lateral moments  $M_n$  of the step meander periods ( $n = 2; 4; 6; 8; 10$  from top to bottom) as a function of coverage in a semi-logarithmic scale. The moments approach constant values already before  $2.0$  ML. (b) Width  $w$  of the profiles as a function of the coverage. No saturation is observed up to  $10$  ML. The slope of the solid line corresponds to  $\alpha = 1/3$ .

meandering of steps begins gradually to phase-lock, seen in Fig. 1 (b), and in-phase growth and phase-locking seem complete at largest studied coverage of  $10$  ML shown in Fig 1 (c). However, now the average shape of the patterns is clearly different from that at low coverages. The shape of the average patterns is more rounded, as predicted for a weak K ESE. In Fig. 1 (d) we show this change by comparing average ledge profiles after  $0.4$  and  $2.0$  ML, respectively<sup>15</sup>.

From Fig. 1 it is clear that there is no coarsening of the structures when the coverage is large enough. The steady state pattern shape seems to be governed by geometric constraints which is a sign of asymmetry of the growth rates between bottom and top parts of the steps. Moreover, a quantitative inspection of the patterns at larger coverages suggest that the profiles have an invariant shape. This can be seen by examining the  $n$ th lateral moments  $M_n(\theta) = \langle h_i(x; \theta)^n \rangle_{i,x}$  of the meander periods  $h_i(x; \theta)$ , shown in Fig. 2 (a). The scaled even moments approach their steady state values already at  $2$  ML. The patterns are still changing, however, which can be seen from the roughness of the step  $w(\theta) = \langle h_i(x; \theta)^2 \rangle_{i,x}$ , where  $\langle \dots \rangle$  is the step profile. It does not show any sign of saturation up to the largest coverage in the simulations. Instead the roughness follows  $w(\theta) \sim \theta^{0.3}$ , with  $0.3$  as shown in Fig. 2 (b). It is interesting to note that although the roughness does not saturate the shape

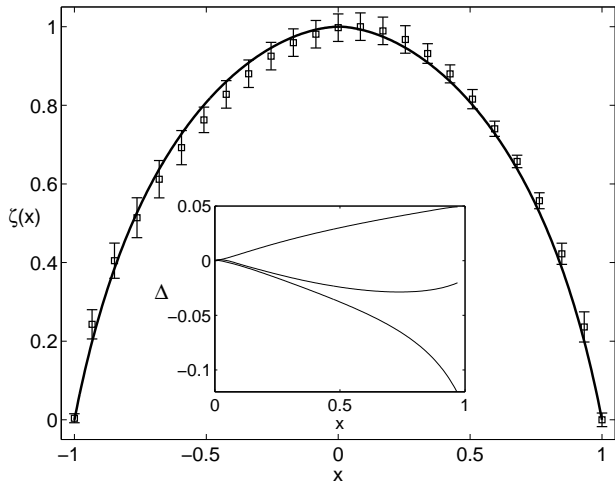


Fig. 3: The average shape of the step patterns at  $T = 300$  K and  $\mu = 8.0$  ML with  $F = 6 \cdot 10^{-2}$  ML/s (squares). Changing the temperature or the flux as described in the text does not have any effects within the error bars. The solid line is the stationary profile obtained by integration of Eq. (5). Good agreement between the average and the integrated profiles is evident. The inset displays the relative differences of the profiles,  $\Delta = (\phi_{\text{all}} - \phi_i) / \phi_{\text{all}}$ , where  $\phi_{\text{all}}$  is the profile with all currents included, and  $i = k; e; SB$  denotes the solution with only a small contribution for the KESSE current from the Gibbs-Thomson and symmetry breaking currents, respectively (from top to bottom in the inset).

of the periodic structures attains an invariant form.

Our simulation results show that the profile shape is rather insensitive to deposition and temperature conditions. This suggests that the invariant shape is not dependent on the relative magnitudes of the various diffusion processes but rather is a result of geometric constraints due to crowding and in-phase evolution of the step edges. In order to justify this assumption we compare the MC profiles with continuum profiles which are obtained as stationary solutions to the dynamic equation  $\partial_t m = \partial_x J_{\text{tot}}$ ; where  $J_{\text{tot}}$  is the total mass current at the step edge. The most important partial currents which we take into account in the total current here, when expressed in terms of the variable  $m(x) = (\partial_x m)^2 / (1 + (\partial_x m)^2)$  and appropriately scaled, are the mass current due to the destabilizing strong KESSE<sup>4</sup>

$$J_k = \frac{m \frac{D_s \tilde{L}}{F} \frac{1}{1 - m^2} (j_n j)}{(j_n j + L_c \frac{1}{F} \frac{1}{1 - m^2})^2}; \quad (1)$$

the stabilizing current due to the Gibbs-Thomson effect and edge diffusion<sup>11;12;16</sup>

$$J_e = \frac{2D_s \tilde{L}}{F} \frac{1}{1 - m^2} + \frac{D_L}{D_s L} (\partial_{xx} m) \frac{1}{1 - m^2}; \quad (2)$$

the current into the step edge from the deposition flux<sup>11;12;16</sup>

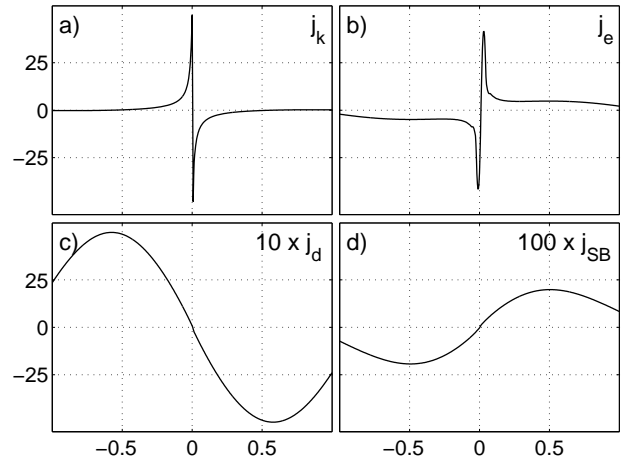


Fig. 4: The mass currents Eqs. (1)–(4) are shown using the integrated profile as an input. Note the difference between the vertical scales for (c) and (d).

$$J_d = L m \frac{1}{1 - m^2}; \quad (3)$$

and the front-back symmetry breaking current<sup>12;17</sup>

$$J_{SB} = \frac{D_s \tilde{L}}{F} (\partial_x m) (\partial_{xx} m) \frac{1}{1 - m^2} + \frac{L^2}{3} m (\partial_x m) (3 - m^2); \quad (4)$$

In these expressions  $L$  is the terrace width,  $D_s$  is the macroscopic diffusion constant on the terrace,  $D_L$  is the macroscopic diffusion constant along the step edge, and  $\tilde{L}$  is the step stiffness (see Refs.<sup>12;18</sup> for the definitions and experimental values of the parameters, respectively). All length scales are given in the units of the lattice constant. By requiring the condition of stationarity

$$J_{\text{tot}} = J_k + J_e + J_d + J_{SB} = 0; \quad (5)$$

we obtain a second order differential equation for  $m(x)$ . The stationary profiles are obtained by solving Eq. (5) numerically for given initial conditions  $m(-1) = m_0$ .

The stationary solution is found using the value  $m_0 = 0.97$  as the boundary condition in order to match the end points with the slopes of the patterns obtained from the MC simulations. The value  $m_0 = 1$  would imply a diverging shape at the end points which is not physically justified. However, by matching the slopes with the MC profiles gives the same results also for  $m_0 = 1$ . The other parameter values of the integration are based on known energetics of Cu, yielding  $\tilde{L} = 700 - 1600$ ,  $\tilde{L}_s = 2 \cdot 10^4 - 2 \cdot 10^5$ ,  $D_L = (D_s L) = 250 - 700$ , and  $D_s \tilde{L} = F = 0.5 - 4000$  in the range  $T = 240 - 300$  K and  $F = 3 \cdot 10^{-3} - 10^{-1}$  ML/s. For the step stiffness we used the expression  $\tilde{L} = \exp[E_k / k_B T] / 2$ , where  $E_k = 0.13$  eV is the kink energy<sup>19</sup>. In all cases we set  $L = 10$  for the terrace width. The resulting profiles are shown in Fig. 3 with various values of the parameters. The shape is rather

independent of the details of the currents in agreement with simulations. In Fig. 3 the average shapes obtained from the simulations are plotted with a few different flux rates. In the inset we show how the resulting profile deviates from the complete one when each of the mass currents is forced to be small.

In Fig. 4 we show the mass currents using the integrated profile as an input. It is now seen that for the invariant profile there is a delicate compensation of the currents, the Gibbs-Thomson current compensated by the sum of the KESE, the deposition, and the symmetry breaking currents. This compensation happens for the specific shape of the profile, and cannot take place e.g. in the case of a triangular shaped profile as obtained in the initial stages of growth. In determination of the stationary profile shape the front-back symmetry breaking and the geometric constraints contained implicitly in the initial conditions are crucial.

In summary, the MC<sup>7</sup> and the SOS<sup>8</sup> simulations have proven that the KESE is the dominant mechanism behind the meandering instability and that it leads to the selection of the dominant wavelength determined by dimer nucleation at step edges. In this work we have shown that the KESE also induces an invariant shape of the step profiles during in-phase growth. This occurs even though the overall roughness of the step structures  $w(\lambda)$  shows no signs of saturation. The value of the corresponding scaling exponent  $\beta = 0.3$  is consistent with the case of an isolated step<sup>20</sup>. The SOS model gives for the strong KESE an exponent  $\beta = 0.57^4$ , while for a collection of steps in the phase-locking regime  $\beta = 1 = 2^{11;12;16}$ . This puzzling behavior of dynamical scaling is apparently related to the strict in-phase growth and consequent formation of the invariant shape of the profile. The fact that the shape remains invariant although the roughness does not show any sign of saturation indicates a subtle coupling of the step edge currents with the stationary morphology. These are aspects not fully described by any existing continuum model. Clearly, the formation of an invariant profile shape demonstrated here by simulations and the related anomaly in scaling deserve more theoretical studies.

Acknowledgements: We wish to thank J. Kallunki and Z. Chvoj for helpful discussions and the Center of Scientific Computing, Ltd. for computing time. TSR and CG thank colleagues at Fyslab, HUT for their wonderful hospitality during their stay in Helsinki. This work has been supported by the Academy of Finland, in part through its Center of Excellence program. We also acknowledge partial support from the National Science Foundation, USA under Grant EEC-0085604 (including International Supplement).

- <sup>1</sup> H.-C. Jeong and E. D. Williams, Surf. Sci. Rep. 34, 171 (1999); P. Politi, G. Grenet, A. Marty, A. Ponchet, and J. Villain, Phys. Rev. Lett. 82, 271 (2000).
- <sup>2</sup> G. Ehrlich and F.G. Hudda, J. Chem. Phys. 44, 1039 (1966); R.L. Schwoebel and E.J. Shipsey, J. Appl. Phys. 37, 3682 (1966).
- <sup>3</sup> G.S. Bales and A. Zangwill, Phys. Rev. B 41, 5500 (1990).
- <sup>4</sup> O. Pierre-Louis, M.R. D'Orsogna, and T.L. Einstein, Phys. Rev. Lett. 82, 3661 (1999).
- <sup>5</sup> L. Schwenger, R.L. Folkerts, and H.J. Ernst, Phys. Rev. B 55, R7406 (1997).
- <sup>6</sup> T.M. Aroutian, L. Douillard, and H.J. Ernst, Phys. Rev. Lett. 83, 4353 (1999); T.M. Aroutian (private communication).
- <sup>7</sup> M. Rusanen, I.T. Kopenen, J. Heinonen, and T. Ala-Nissila, Phys. Rev. Lett. 86, 5317 (2001).
- <sup>8</sup> J. Kallunki, J. K rug, and M. Kotrla, e-print cond-mat/0108059.
- <sup>9</sup> M.V. Ramana Murty and B.H. Cooper, Phys. Rev. Lett. 83, 352 (1999).
- <sup>10</sup> P. Politi, J. Phys. I (France) 7, 797 (1997); J. K rug and M. Schimsak, J. Phys. I (France) 5, 1065 (1995).
- <sup>11</sup> O. Pierre-Louis, C.M. Isbah, Y. Saito, J. K rug, and P. Politi, Phys. Rev. Lett. 80, 4221 (1998).
- <sup>12</sup> F. Gillet, O. Pierre-Louis, and C.M. Isbah, Eur. Phys. J. B 18, 519 (2000).
- <sup>13</sup> J. Heinonen, I. Kopenen, J. Merikoski, and T. Ala-Nissila, Phys. Rev. Lett. 82, 2733 (1999).
- <sup>14</sup> J. K rug, Adv. Phys. 46, 139 (1997).
- <sup>15</sup> The profiles have been obtained by averaging over the meander periods  $\lambda_i(x; \lambda)$  and scaling each period as  $\lambda_i = \lambda \cdot \frac{\lambda_i}{\lambda}$ , where  $\lambda_i$  is the wavelength of the period along the step direction,  $\lambda$  is the wavelength of the period, and  $w(\lambda)$  is the roughness.
- <sup>16</sup> J. Kallunki and J. K rug, Phys. Rev. E 62, 6229 (2000).
- <sup>17</sup> P. Politi and J. Villain, Phys. Rev. B 54, 5114 (1996); I. Elkinani and J. Villain, J. Phys. I (France) 1, 1991 (1994).
- <sup>18</sup> M. Giesen, Prog. Surf. Sci. 68, 1 (2001).
- <sup>19</sup> M. Giesen-Seibert, R. Jentjens, M. Poensgen, and H. Ibach, Phys. Rev. Lett. 71, 3521 (1993); M. Giesen-Seibert, F. Schmitz, R. Jentjens, and H. Ibach, Surf. Sci. 329, 47 (1993).
- <sup>20</sup> T. Sakitt and H. Spohn, Phys. Rev. E 47, 3524 (1993).